Homing Radar Tracking Accuracy Improvement with Frequency Diversity

P. JONES,* E. A. MICKLE,† AND G. D. SWETNAM‡
The Boeing Company, Kent, Wash.

Available theory concerning glint reduction by usage of frequency diversity in a radar tracker is reviewed and unified. The theory was verified experimentally using 1) a target consisting of two corner reflectors (which could be representative of a low-flying aircraft and its sea image), 2) an isolated aircraft in level flight, and 3) a boat in a sea-clutter background. A simulation was used to reflect this glint reduction into a reduction of miss distance. The rms miss is reduced by as much as a factor of three corresponding to usage of nine carrier frequencies.

Nomenclature

A = commanded acceleration
Az = azimuth
B = diversity bandwidth
C = clutter power
c = speed of light
EL = elevation
f = frequency
f_γ = half-power frequency of power spectral density of target glint
Δf = frequency change
Δf_D = critical frequency change
I = improvement factor
j = summing index
k = voltage amplitude ratio for the two-reflector target
K_1,K_2,K_3,K_4 = noise scaling constants (Fig. 2)
L = target length normal to the line of sight
N = actual number of pulses integrated
N_e = equivalent number of independent pulses integrated, contained in N
N_{e1} = equivalent number of independent pulses integrated, contained in N for an an isolated target with monofrequency operation
N_{e2} = equivalent number of independent pulses integrated, contained in N for an isolated target with frequency diversity operation
N_{e3} = equivalent number of independent pulses integrated, contained in N for a target embedded in clutter with monofrequency operation
N_{e4} = equivalent number of independent pulses integrated, contained in N for target embedded in clutter with frequency diversity operation
N_F = number of frequencies in one period of frequency diversity schedule
$N_G{}^2$ = spectral density of the target glint at a reference range
$r_t(j)$ = the correlation coefficient of the return on a given pulse with the return on a pulse spaced jT away due only to the time separation of the pulses
$r_f(j)$ = the correlation coefficient of the return on a given pulse with the return on a pulse spaced jT away due only to the frequency difference between the two transmitted carrier frequencies of the pulses
R = range from radar to target
R_T = range depth of the target or extent of the range gate, whichever is smaller
$\dot{R}$ = rate of change of R
S = target signal power in the radar
s = Laplacian variable
t = time
Δt = time separation between frequency changes
t_i = radar post-detection integration time
T = interpulse period
α = angle subtended by the target at the radar (Fig. 6)
β = one-way half-power beamwidth of the tracking antenna
ν = guidance constant
θ_{0m} = maximum observable glint angle with monofrequency operation
θ_{0f} = observable glint angle with frequency diversity operation
σ = standard deviation
Σ = summation symbol
$d\sigma^2$ = variance of quantity identified by subscript using frequency diversity
$m\sigma^2$ = variance of quantity identified by subscript using fixed frequency operation
$\tau_1,\tau_2,\tau_3,\tau_4$ = noise time constants (Fig. 2)
τ_c = correlation time
ϕ = phase difference of the signals received from two reflectors
$\dot{\psi}$ = rate of change of line of sight referred to inertial coordinates.

Presented as Paper 70-992 at the AIAA Guidance, Control and Flight Mechanics Conference, Santa Barbara, Calif., August 17–19, 1970; submitted September 9, 1970; revision received May 12, 1971.

* Research Specialist, Aerospace Group. Member AIAA.
† Research Specialist, Aerospace Groups.
‡ Manager of Guidance Research, Aerospace Group.

Introduction

PROPORTIONAL guidance is widely used in non-nuclear homing-guided missiles. This type of guidance is of the form

$$A = \delta \dot{R} \dot{\psi} \tag{1}$$

where δ is built into the system, and $\dot{R}$ and $\dot{\psi}$ are sensed by a homing sensor or tracker during intercept.

Errors in A result from two major sources: 1) imperfections in equipment manufacture and 2) target tracking noise. The first error source results from hardware drifts, hardware tolerances, and imperfect hardware alignments. In principle, these error sources may be reduced to any desired level by design and manufacturing techniques. The second error source, however, is a strong function of the homing sensor used to sense the target position with respect to the missile.

Single-frequency radar trackers suffer from a disturbing phenomenon known as glint which results from interference between the electromagnetic waves reflected from different parts of a complex target. The effect of this glint is to blur our knowledge of $\dot{R}$ and $\dot{\psi}$.

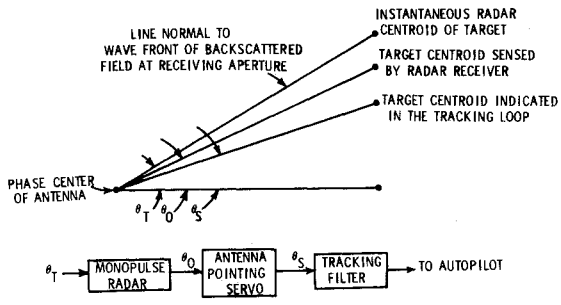

Fig. 1 True, observed, and system glint.

There are several angular errors existing at different points in the missile's guidance subsystem that are collectively referred to as glint. These are distinguished by the terms true glint, observable glint, and system glint (see Fig. 1). True glint θ_T is the angle between a line from the phase center of the homer's antenna to the geometric centroid of the target and a line normal to the wavefront of the back-scattered field from the target at the phase center of the receiving aperture. Observable glint θ_0 is the angular error signal at the output of the receiver caused by true glint introduced at the aperture of the sensor's antenna. Observable glint is different from true glint principally because of post-detection integration of the receiver. System glint θ_S is the angular error signal in the missile's tracking loop caused by true glint introduced at the sensor's aperture. System glint includes the integrating effect and lag introduced by the servo that points the antenna. In an operational situation, θ_0 and θ_s are referenced to the sensor's boresight.

The guidance simulation[2] used in this study is shown in Fig. 2. Random number tables are sampled as the starting point in generating both range glint and angle glint referred to a reference range. Range dependence is then inserted after the first-order filter, which is used to scale the variance of the sampled random numbers and is select the correlation time to agree with experimental measurements. The final step is differentiation, since range rate and angular rate are used in the proportional guidance law, and the noisy rates are then added to the signal rate.

The simulation employs a Monte Carlo technique yielding one estimate of miss distance for each terminal engagement simulated. A large number of repetitions of a specified engagement produces a stable estimate of the root-mean-square miss distance. The confidence bounds on the estimate can be evaluated as a function of the number of repetitions from standard statistical theory.

Typical simulation results with the assumptions of the preceding paragraphs are shown in Fig. 3, which presents the rms miss distance as a function of the rms observable glint for single isolated aircraft targets. The miss distance for zero glint results from range independent noises such as range and angle servo jitter.

Frequency diversity is a method for reducing the effects of glint. It does this by changing the frequency of the transmitted signal rapidly with respect to the filters in the radar, antenna pointing servo, and tracking filter. The maximum deviation of frequency is limited to some bandwidth called the frequency-diversity bandwidth. The particular sequence of discrete frequencies within this bandwidth may be selected on either a random§ or deterministic basis. Figure 4 indicates a commonly used deterministic selection.

Frequency change introduces change in glint by changing the number of wavelengths in the ranges to the reflectors composing the target. This causes the relative phases of the received signals from the reflectors to change, thereby shifting the position of the instantaneous radar centroid. The instantaneous radar centroids are averaged over the radar's post-detection integration interval to produce an observable radar centroid. Further averaging is applied by the antenna pointing servo to produce system glint, which directly affects the missile's commanded acceleration. The tracking filter may provide further smoothing.

Figure 5 shows the transmitted pulse train and defines some pertinent symbols needed to derive a figure of merit or improvement factor for frequency diversity.

Theory

Two-Reflector Target

The two-reflector target is a useful model for developing a theoretical understanding of glint because of its simplicity. It also represents a severe illustration of glint excursions when the returns from the two reflectors are nearly equal in amplitude and approximately 180° out of phase. Another interesting feature of this model is that true glint, considered as a function of relative phase of the two received voltages, is a deterministic period function rather than a random process. Our studies have shown that deterministic glint requires a schedule of frequencies different from the schedule required for reducing random glint by means of frequency diversity.

With the sign convention indicated in Fig. 6, θ_T is expressed in terms of α, k, and ϕ by [3-5]

$$\theta_T = \alpha(1 - k^2)/[2(k^2 + 2k\cos\phi + 1)], \quad 0 < k < 1 \qquad (2)$$

The probability that, at a randomly chosen observation time, the instantaneous radar centroid lies outside the physical dimensions of the two-element target is shown as a function of k in Fig. 7. This assumes that all relative phase angles are equally likely and neglects the smoothing effect of integration of the received signal across the receiving aperture. Averaging over k, we find that 28% of the time the instantaneous radar centroid lies outside the physical limits of the two-point target. This is more severe than for a linear array of N equal reflectors ($N \geq 5$), which is shown for comparison.

The glint error is proportional to the target length normal to the line of sight from the radar and inversely proportional to the missile-target range. Thus, glint error becomes more important as the missile closes on the target.

If the geometry and carrier frequency are fixed, the true glint angle is a constant since α, k, and ϕ are also fixed. In this case the post-detection integration performed in the receiver does no averaging so that θ_0 is identical to θ_T. Now suppose that the radar is operated in the frequency-diverse mode and that the diversity bandwidth is sufficient to change the relative phase angle by one full cycle. Pulses using different carrier frequencies within this bandwidth produce samples of θ_T at different values of ϕ over one complete cycle of glint ($0 \leq \phi \leq 2\pi$). The post-detection integration of N pulses then produces a sample average of θ_T considered as a function of ϕ. If a large number of discrete frequencies uniformly spaced over the diversity bandwidth are used, the sample average is nearly identical to the theoretical average. The theoretical average can be determined from Eq. (2) by integration with respect to ϕ:

$$\langle\theta_T(\phi)\rangle = \alpha/2, \; 0 < k < 1 \qquad (3)$$

We define the improvement factor for the deterministic two-reflector target as follows:

$$I = \theta_{0m}/\theta_{0f} = \theta_{0m}/\langle\theta_T(\phi)\rangle = (1 + k)/(1 - k) \qquad (4)$$

§ The random selection of frequencies has an advantage in an ECM environment. Lind[10] treats this case in detail and distinguishes it from deterministic selection by calling it "frequency agility" as compared to frequency diversity.

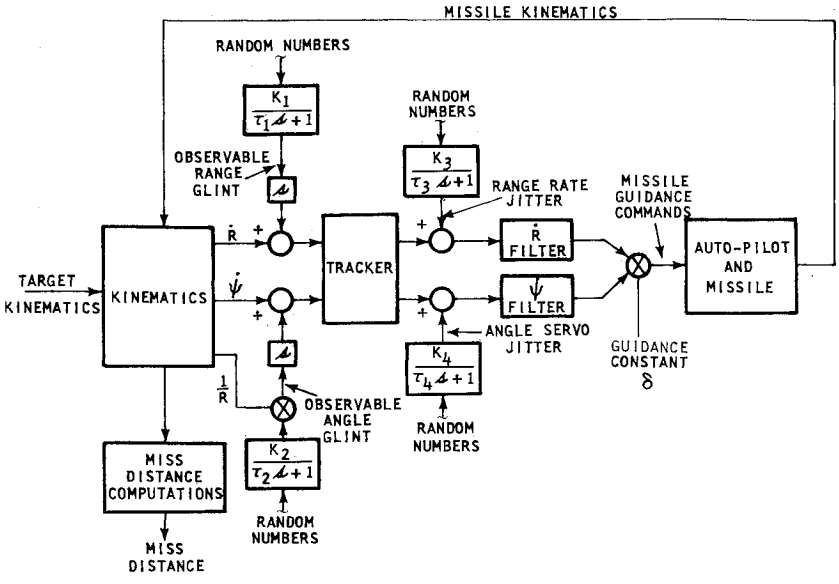

Fig. 2 Guidance simulation.

This represents the theoretical maximum improvement achievable from frequency diversity, referenced to the line to the geometric centroid between the two reflectors.

The two-reflector target has been studied primarily for theoretical interest. However, it sometimes provides a good approximation in practical situations. For example, it is a good model for two targets located within the same radar-resolution cell or for the low-angle tracking situation in which the radar sees the target plus its image reflected from the surface. For these situations the geometric centroid between the two reflectors is not the desired homing point. Rather, the desired homing point is the reflector that provides the larger voltage return at the radar. (Here we assume that a target will generally provide a larger return than its image in the low-angle tracking situation, at least over an averaging interval equal to the post-detection integration time of the receiver.)

Equation (4) does not represent the two-reflector target as a model for these two practical situations because it is based on the desirability of homing on the geometric centroid. The desired homing point is the larger reflector in this case, and, fortunately, this is the average position of the radar centroid, as indicated by Eq. (3). Frequency diversity coupled with post-detection integration provides an approximation to the average with respect to ϕ.

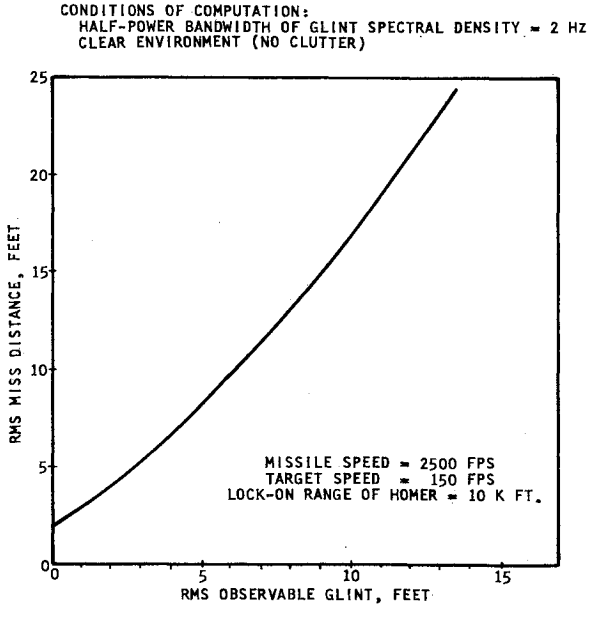

Fig. 3 Rms miss distance vs rms observable angular glint.

Aircraft Target

On the basis of empirical evidence, we describe the monofrequency spectral density of the glint noise (at a reference range) as follows:

$$N_G^2 = (3.5)(10)^{-3}L^2/[1 + (f/f_\gamma)^2] \tag{5}$$

The value of f_γ must be determined empirically for different targets. One way to do this is to measure the mean square glint $\langle N_G^2 \rangle$ and then to compute f_γ from relation (6):

$$f_\gamma = \langle N_G^2 \rangle/[(\pi/2)(3.5)(10)^{-3}L^2] \tag{6}$$

For several aircraft targets f_γ is about two Hertz.[9] The glint spectral density given by Eq. (5) is passed through a kinematic filter to introduce the inverse dependence on range in the terminal guidance simulation.

The observable glint is related to the set of true glint samples $\theta_{T,j}$ by

$$\theta_0 = \frac{1}{N}\sum_{j=1}^{N} \theta_{T,j} \tag{7}$$

The true glint samples are regarded as samples from a stationary random process. Then within the set of N samples, there will be an equivalent of N_e statistically independent samples. The variance of θ_0 is related to the variance of θ_T by

$$\sigma_{\theta_0}^2 = \sigma_{\theta T}^2/N_e \tag{8}$$

The value of N_e is influenced only by time decorrelation when monofrequency operation is used,[11,13] but when fre-

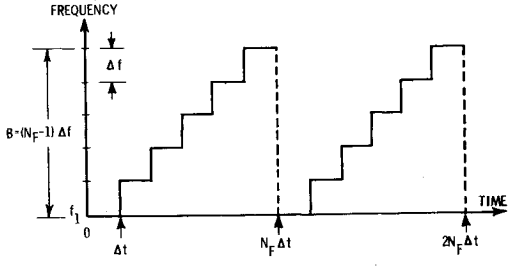

Fig. 4 Frequency schedule for uniform time and uniform frequency jumps, repeated cyclically.

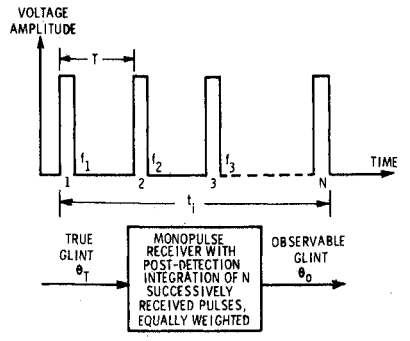

Fig. 5 Transmitted pulse train, input and output of receiver.

quency-diverse operation is employed, N_e depends on both time and frequency decorrelation[11-14]:

$$N_{e1} = N \Big/ \left[1 + 2 \sum_{j=1}^{N-1} \frac{N-j}{N} r_t(j)\right]$$

$$N_{e2} = N \Big/ \left[1 + 2 \sum_{j=1}^{N-1} \frac{N-j}{N} r_t(j) r_f(j)\right] \tag{9}$$

The improvement I, due to frequency diversity, is defined as the ratio of the standard deviation of observable glint when monofrequency transmission is used to the standard deviation of observable glint when frequency-diverse transmission is used:

$$I = \left[\left\{1 + 2 \sum_{j=1}^{N-1} \frac{N-j}{N} r_t(j)\right\} \Big/ \left\{1 + 2 \sum_{j=1}^{N-1} \frac{N-j}{N} r_t(j) r_f(j)\right\}\right]^{1/2} \tag{10}$$

Maximum improvement occurs when $\tau_c \gg t_i$, in which case Eq. (10) simplifies to Eq. (11):

$$I = N_{e2}^{1/2}, \quad \tau_c \gg t_i \tag{11}$$

This corresponds to $r_f(j) = 0$ for all j and $r_t(j) = 1$ for all j. All $r_f(j)$'s can be zero only if the frequency step size is at least equal to some critical frequency change Δf_D. The critical frequency change Δf_D is defined as the minimum frequency change necessary to produce independent samples of θ_T. For a rod-type target of range depth R_T, the critical frequency change is given by[11]

$$\Delta f_D = c/2R_T \tag{12}$$

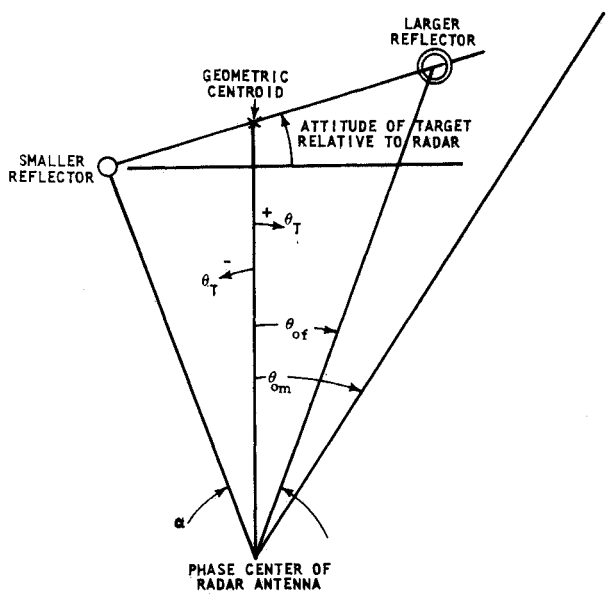

Fig. 6 Quantities pertinent to the two-reflector model.

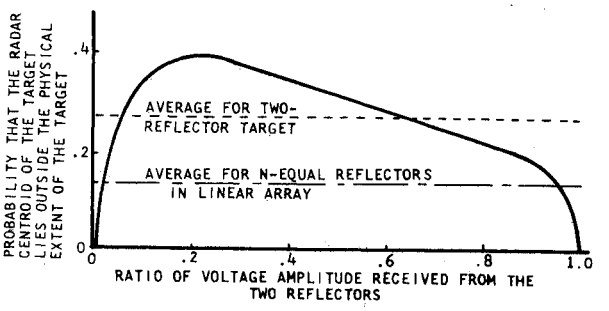

Fig. 7 Probability that the instantaneous radar centroid lies outside the physical limits of two-point target.

Small Boat Target

True glint from a small boat is assumed to be adequately modeled as a stationary random process over the post-detection interval of the radar receiver, as in the case of the aircraft target. But sea clutter complicates the theory since it can significantly affect the angular error out of the integrator.

It is reasonable to treat angular error due to glint and angular error due to clutter as statistically independent since they are produced by reflections from different physical surfaces. The resultant angular error variance at the integrator output is therefore assumed to be equal to the sum of the variance caused by target glint and the variance caused by clutter.

The variance of angular error caused by clutter is related to signal-to-clutter power ratio at the output of the integrator by[3]

$$\sigma_C^2 = 0.25\beta^2/(S/C)_0 \tag{13}$$

The signal-to-clutter ratio out of the integrator is related to that at the input by[13,14]

$$(S/C)_0 = N_e(S/C)_i \tag{14}$$

Here, N_e is the effective number of independent clutter samples contained in the N pulses that are integrated. This value is generally different from the value applicable to the glint. Formula (12) gives the frequency change needed to decorrelate successive clutter returns if R_T is the width of the range gate.

The improvement factor I, due to frequency diversity, is defined as the ratio of the standard deviation of total angular error at the output of the integrator using monofrequency operation to the standard deviation of total angular error using frequency-diverse operation:

$$I = \left[\frac{1}{N_{e3}}\left(\sigma_{\theta T}^2 + \frac{0.25\beta^2}{(S/C)_i}\right) \Big/ \frac{1}{N_{e4}}\left(\sigma_{\theta T}^2 + \frac{0.25\beta^2}{(S/C)_i}\right)\right]^{1/2} = \left(\frac{N_{e4}}{N_{e3}}\right)^{1/2} \tag{15}$$

Equation (15) indicates that frequency diversity acts to reduce both glint-produced angular noise and clutter-produced angular noise by the same averaging mechanism. If the correlation times of both clutter and glint are long relative to the integration time, then N_{e3} is unity and Eq. (15) reduces to the following:

$$I = N_{e4}^{1/2} \tag{16}$$

If the frequency jumps are equally successful in producing independent samples of both glint and clutter, then N_{e4} will be equal to N_{e2} [Eq. (11)]. When this condition occurs, the

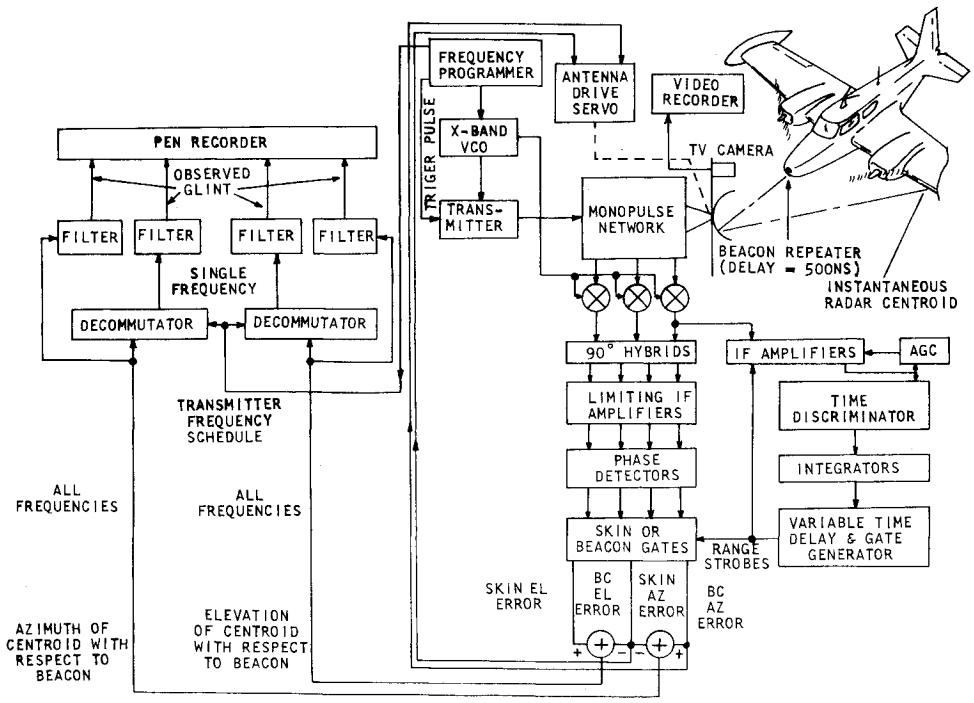

Fig. 8 Simplified block diagram of test radar.

improvement factor is the same in a clutter environment as in a clear environment. In general we suspect that $N_{e4} < N_{e2}$ so that the improvement will be lower in a clutter environment than in a clear environment.

Table 1 Specifications of subsystems of test radar

Antenna and gimbal system	
Type:	parabolic dish
Polarization:	horizontal
Beamwidth:	5°
Feed:	four horn monopulse
Gimbal drive:	hydraulic
Gain:	32 db
Transmitter	
Tuning range:	9.2–9.92 GHz
Peak power:	1 kw max (adjustable)
Burst time:	25 μsec to 51.2 msec in steps, or any one freq. indefinitely
PRF:	40 kHz
Average power:	6 w
Pulse width:	150 nsec
Tube type:	TWT
No. of frequencies:	9
Frequency steps:	8–80 MHz (adjustable)
Receiver	
Type:	single conversion superheterodyne
IF center frequency:	60 MHz
IF bandwidth:	25 MHz
Angle demodulator	
Monopulse types:	4 channel, limiting IF
Range unit	
Type:	early and late gate
Servo:	type II
Early and late gate pulse width:	75 nsec
TV system	
Mount:	on antenna reflector
Tube:	0.5-in. vidicon
Lens focal length:	75 mm
Aircraft beacon	
Type:	repeater
Power peak:	2 w
Pulse width:	150 nsec
Pulse delay time:	500 nsec
Tube type:	TWT
Antenna type:	horn
Antenna beam-width:	28° × 39°

Test Radar Characteristics

A simplified block diagram of the test radar is shown in Fig. 8. The transmitter can be operated in single frequency, pulse-to-pulse frequency diversity, or burst-to-burst frequency diversity modes. The beacon, installed on the target, delays and repeats the received transmission. The beacon return is delayed and the time separation between the skin and beacon returns allows the angles between 1) antenna boresight and beacon and 2) antenna boresight and skin to be measured almost simultaneously by the monopulse receiver. The beacon angle is used to control the antenna servo, resulting in the antenna accurately tracking the beacon position. The angle between the beacon and the skin is fed to the data recording and reduction equipment to obtain the angle glint data.

The specifications of the test radar are shown in Table 1.[15,16]

Tests and Results

Two-Reflector Target

The test setup is shown in Fig. 9. The two reflectors were placed at the angle giving maximum glint, and the glint angle was measured for fixed frequency and frequency diversity. Figure 10 shows the results. Equation (4) was used for the theoretical curves.

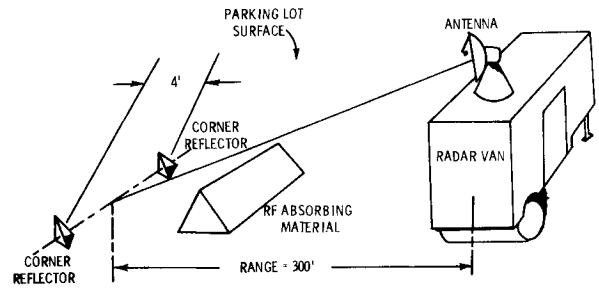

Fig. 9 Test setup for two-reflector target.

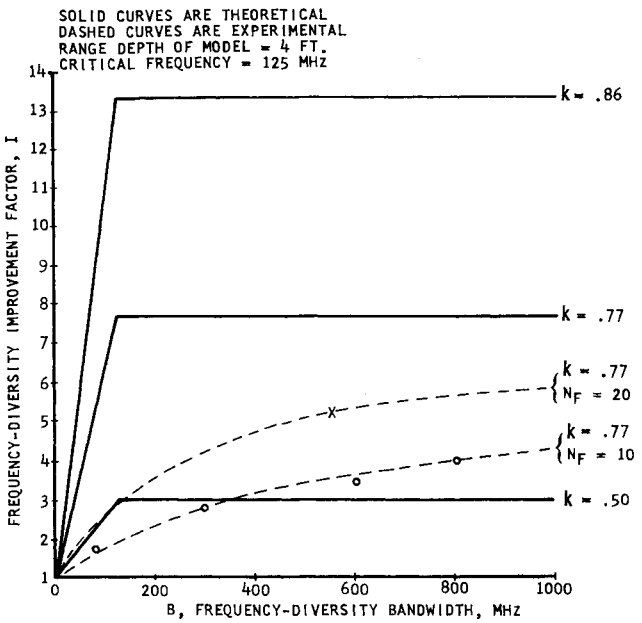

Fig. 10 Theoretical and experimental improvement factor for two-reflector target.

Aircraft Target

Figures 11 shows the results for the aircraft target. Equation (11) was used for the maximum theoretical improvement. The assumed critical frequency change of 20 MHz gives good agreement with experimental evidence.

Small Boat Target

Figure 12 shows the results for the small boat target. The theory did not include bias effects such as the wake of the boat. The magnitude of this effect was surprising, and, in some cases, dominated the angular tracking error.

For a slow moving boat with little or no wake, the improvement factor is 1.5 for $\Delta f = 80$ MHz and 9 frequencies. For a fast moving boat with significant wake, the improvement factor is 2.85. Large wakes cause a bias in the radar centroid

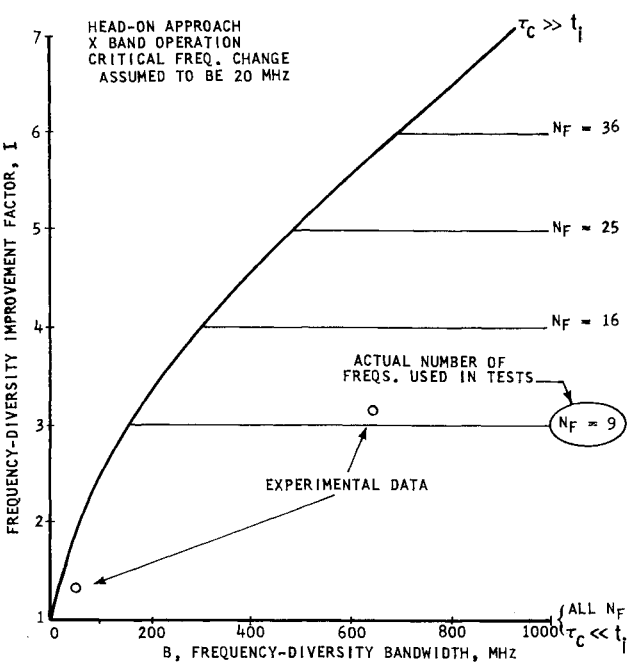

Fig. 11 Theoretical and experimental glint improvement factor for piper comanche aircraft.

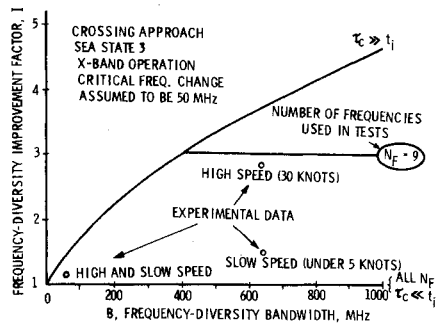

Fig. 12 Theoretical and experimental glint improvement factor for the small boat target.

and for the boat tested at about 30 knots this bias is about 15.6 ft.

Summary and Conclusions

The theory was used to predict the glint improvement factor I as a function of the frequency-diversity bandwidth of the radar for each of the three test targets. Figures 10–12 show a comparison of these theoretical predictions with experimental data. Good agreement between theory and experiment is observed for the Piper Comanche aircraft and the small boat at low speeds using the 80 MHz frequency steps. This indicates that 80 MHz is equal to or greater than the critical frequency change for these targets, whereas 8 MHz steps are below the critical frequency. In the case of the high-speed ship at a crossing approach, the theory does not account for the effects of the wake, which were found experimentally to be very significant.

Experimental evidence indicates that the correlation time of glint (and of sea clutter, in the case of the small-boat target) is long compared to the post-detection integration time of the radar. If this were not the case, little improvement would be observed by usage of frequency diversity. The experiments clearly show that observable glint is significantly reduced by the averaging effect of post-detection integration when frequency diversity is used, whether the true glint is basically a random process or a deterministic function, as in the case of the two-reflector target. The random and deterministic cases call for different schedules of frequency, however. When true glint is random, each frequency jump should equal the critical frequency change, and the improvement factor continues to increase as long as the frequency-diversity bandwidth is increased. When true glint is deterministic, there is no advantage to increasing the frequency-diversity bandwidth beyond the critical frequency change. Within this band, as many frequencies as practically feasible should be used in order to make the sample average a good approximation of the theoretical average of true glint over one cycle of relative phase angle. Experimental results indicate that the use of ten carrier frequencies yields about 40% of the theoretical maximum averaging effect whereas usage of

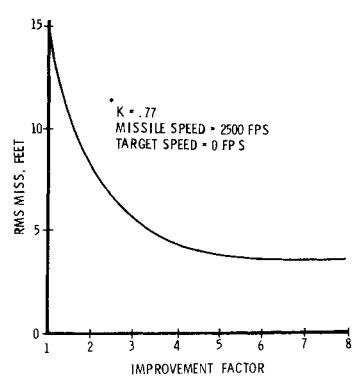

Fig. 13 Rms miss vs improvement for two-reflector target.

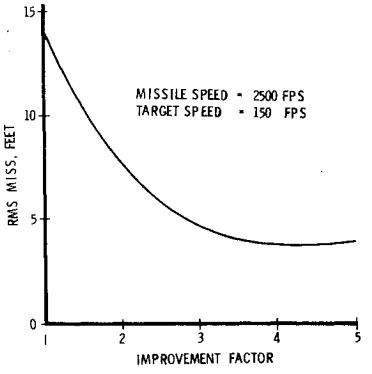

Fig. 14 Rms miss vs improvement factor for aircraft target.

20 frequencies gives about 60% of the theoretical maximum averaging effect (Fig. 10).

Frequency diversity acts to reduce both glint-produced angular noise and clutter-produced angular noise by the same averaging mechanism. For a given schedule of frequencies, the effective number of independent clutter samples will generally be different from the effective number of independent glint samples; the frequency schedule that minimizes the total angular error variance must be determined by trial and error.

The impact of glint reduction on weapon system performance has been estimated by employing the guidance simulation shown in Fig. 2 to obtain miss distance as a function of I. The resulting decrease in miss distance as I increases is strongly influenced by the missile and target dynamics assumed in the terminal guidance simulation. The results are shown in Figs. 13–15. They are based on the characteristics of a missile carrying an active radar seeker which acquires the target at a range of 10,000 ft.

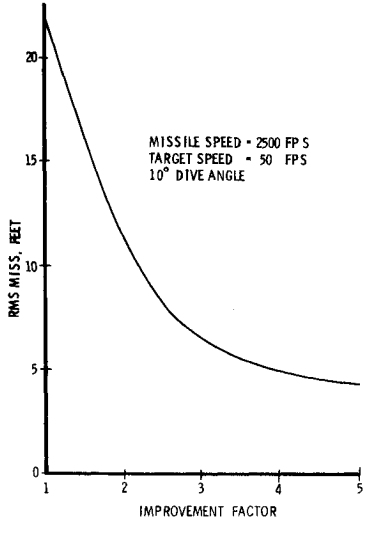

Fig. 15 Rms miss vs improvement factor for small boat target.

References

[1] Havens, W. J., Mickle, E. A., and Swetnam, G. D., "Payload Effectiveness—1969," Document D2-121737-1, Feb. 1970, The Boeing Co., Kent, Wash.

[2] Havens, W. F., "TERMGUID Simulation Program," Document D2-121736-1, March 1970, The Boeing Co., Kent, Wash.

[3] Barton, D. K., *Radar System Analysis*, Prentice-Hall, Englewood Cliffs, N. J., 1964.

[4] Skolnik, M. I., *Introduction to Radar Systems*, McGraw-Hill, New York, 1962.

[5] Meade, J. E., "Target Considerations," *Guidance*, edited by A. S. Locke et al., Van Nostrand, Princeton, N. J., 1955, Chap. 11, pp. 420–442.

[6] Howard, D. D., "Radar Target Angular Scintillation in Tracking and Guidance Systems Based on Echo Signal Phase Front Distortion," *Proceedings National Electronics Conference*, Vol. 15, Oct. 1959, pp. 840–849.

[7] Dunn, J. H., Howard, D. D., and King, A. M., "Phenomena of Scintillation Noise in Radar Tracking Systems," *Proceedings of the IRE*, Vol. 47, May 1959, pp. 855–863.

[8] Mickle, E. A., "Three-Reflector Glint Model," Memo 2-5480-20-380, April 1969, The Boeing Co., Kent, Wash.

[9] Gabler, R. T., "An Estimate of Glint Noise From Radar Tracking Data," RM-683, Sept. 1951, Rand Corp., Los Angeles, Calif.

[10] Lind, G., "Reduction of Radar Tracking Errors with Frequency Agility," *IEEE Transactions on Aerospace and Electronic Systems*, Vol. AES-4, No. 3, May 1968, pp. 410–416.

[11] Birkemeier, W. P. and Wallace, N. D., "Radar Tracking Accuracy Improvement by Means of Pulse-to-Pulse Frequency Modulation," *AIEE Transactions on Communications and Electronics*, Vol. 81, Jan. 1963, pp. 571–575.

[12] Mickle, E. A., "Enhancement of Radar Tracking Accuracy by Frequency Modulation of the Carrier," Memo 2-5482-41-013, May 1969, The Boeing Co., Kent, Wash.

[13] Beasley, E. W. and Ward, H. R., "A Quantitative Analysis of Sea Clutter Decorrelation with Frequency Agility," *IEEE Transactions on Aerospace and Electronics Systems*, Vol. AES-4, No. 3, May 1968, pp. 468–473.

[14] Lind, G., "Measurement of Sea Clutter Correlation with Frequency Agility and Fixed Frequency Radar," Abstract, Philips Teleindustri, Stockholm, Sweden.

[15] Cofield, D. H., "Frequency Diversity/Glint Measurement Radar," Document D2-121735-1, April 1970, The Boeing Co., Kent, Wash.

[16] Schwarzkopf, D., "A High Precision Monopulse Receiver," *Microwave Journal*, Aug. 1967, pp. 92–101.